J Neural Transm (2007) 114: 577–584
DOI 10.1007/s00702-006-0610-7
Printed in the Netherlands

Journal of Neural Transmission

Association of vascular parkinsonism with impaired neuronal integrity in the striatum

M. Ihara[1], H. Tomimoto[1], K. Ishizu[2], H. Yoshida[3], N. Sawamoto[3], K. Hashikawa[3], H. Fukuyama[3]

[1] Department of Neurology, Kyoto University Graduate School of Medicine, Kyoto, Japan
[2] Nuclear Medicine and Diagnostic Radiology, Kyoto University Graduate School of Medicine, Kyoto, Japan
[3] Human Brain Research Center, Kyoto University Graduate School of Medicine, Kyoto, Japan

Received: May 23, 2006 / Accepted: November 14, 2006 / Published online: January 18, 2007

Summary The purpose of this study is to identify the underlying differences between patients with white matter lesions (WMLs) who manifested gait disturbance suggestive of vascular parkinsonism (VaP) and those who did not, using the PET scan. Fourteen patients with extensive WMLs, as determined by MRI, were divided into two groups – 7 with gait disturbance and 7 without it. Neuronal integrity was evaluated with a PET scan using [^{11}C]flumazenil (FMZ) by calculating the distribution volume of FMZ (FMZ-V_d) in various regions of interest by non-linear curve fitting. Additionally, tracer kinetic analysis was applied for voxel-by-voxel quantification of FMZ-V_d and data analysis was performed using statistical parametric mapping. The striatal FMZ-V_d values were inversely correlated with the motor UPDRS scores ($r = 0.70$, $p < 0.005$), and their reductions were associated with the presence of gait disturbance. Therefore, differences in neuronal integrity in the striatum may determine whether patients with WMLs develop VaP or not.

Keywords: Vascular parkinsonism, flumazenil, striatum, white matter, small vessel disease

Introduction

Vascular parkinsonism (VaP) develops as a consequence of heterogeneous groups of cerebrovascular diseases (Winikates and Jankovic, 1999; Sibon et al., 2004; Ebersbach and Poewe, 2006). The incidence of VaP is reported to be 3.4% in an autopsy series of 759 patients with clinical parkinsonism (Jellinger, 2003). VaP primarily affects the lower body and is characterized by a poor response to levodopa, suggesting that it has a different pathophysiology than idiopathic Parkinson's disease (IPD) (van Zagten et al., 1998; Winikates and Jankovic, 1999; Foltynie et al., 2002; Sibon et al., 2004; Rampello et al., 2005). Although striatal lacunar infarcts have been thought to cause VaP (Zijlmans et al., 1995), a meta-analysis revealed that only 9% of patients with these lesions developed parkinsonism (Foltynie et al., 2002); one group even reported an absence of a correlation between the two conditions (Bhatia and Marsden, 1994). Furthermore, a clinicopathological study suggested that white matter lesions (WMLs) rather than striatal lacunar infarcts were the more direct cause of VaP (Yamanouchi and Nagura, 1997). Inconsistencies between these studies may have, at least partially, been due to the heterogenous features of stroke patients.

In this study, we sought to identify the underlying differences between patients with WMLs who manifested gait disturbance suggestive of VaP and those who did not, using the PET scan. Since varying degrees of WMLs and striatal lacunar infarcts are seen heterogeneously in patients with small vessel disease (Yamanouchi and Nagura, 1997), we exclusively enrolled patients who exhibited extensive WMLs in order to minimize these differences. We specifically used the central benzodiazepine receptor (BZR) ligand [^{11}C]-flumazenil (FMZ) as a PET tracer, since this ligand was reported to bind to gamma-aminobutyric acid type A ($GABA_A$) receptors that are widely expressed on cerebral neurons (Olsen, 1981) and as such, can be used to assess the integrity of neurons (Heiss et al., 1998; Ihara et al., 2001, 2004). We also examined cerebral blood flow (CBF), cerebral metabolic rate of oxygen metabolism ($CMRO_2$), and the oxygen extraction fraction (OEF) using the ^{15}O gas steady-state method.

Correspondence: Masafumi Ihara, MD, PhD, Department of Neurology, Kyoto University Graduate School of Medicine, Shogoin, Sakyo, Kyoto 606-8507, Japan
e-mail: ihara@kuhp.kyoto-u.ac.jp

Material and methods

Patients

Fourteen patients whose T2-weighted MRI scans revealed confluent hyperintensities in the subcortical white matter (Schmidt scale score of 3) (Schmidt et al., 1996), as determined at our Neurology Clinic from May 1999 to March 2005, as well as several punctate high-intensity areas in the striatum and/or thalamus were enrolled independently of their clinical status and subjected to PET scanning (Fig. 1). Each subject was fully informed about the experimental procedures and provided written, informed consent; their inclusion in this study was approved by the Ethical Committee

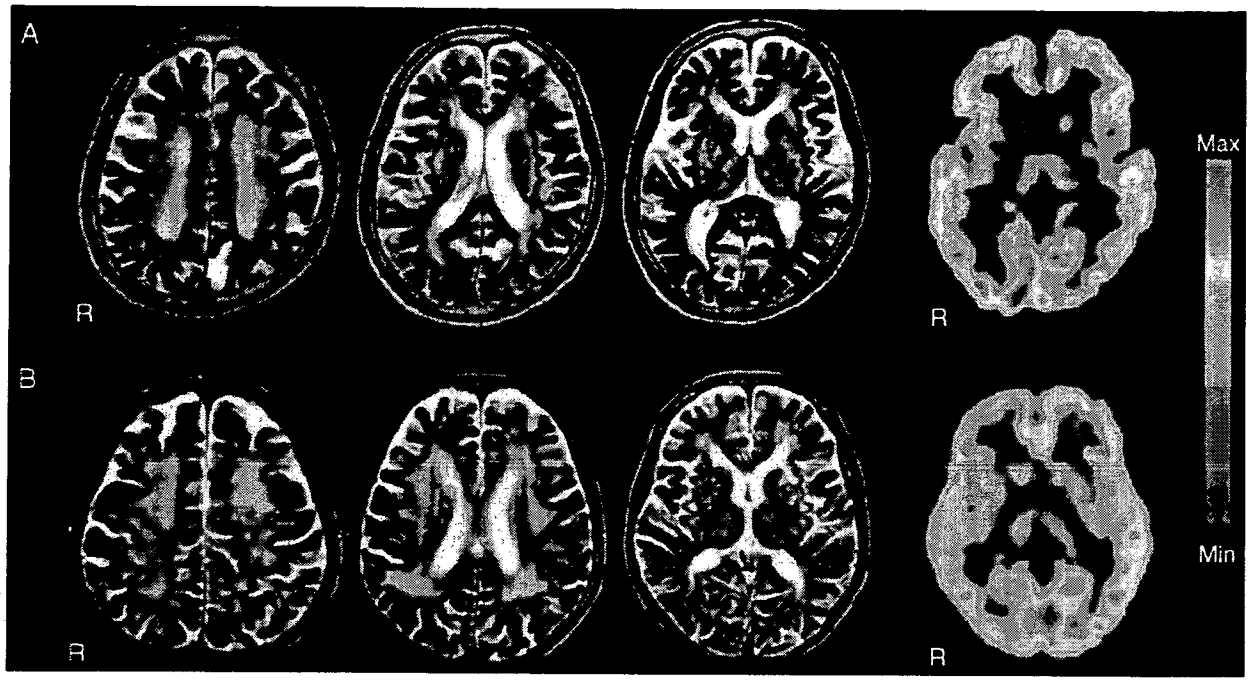

Fig. 1. Representative T2-weighted MRIs and parametric PET images of FMZ-V_d in two patients with WMLs (**A**, gait disturbance; **B**, no gait disturbance). FMZ-V_d values are noted in the pseudocolor scale ranging from 0 to 10 ml/gm. *R* indicates right

Table 1. Demographic features of the patients

Variable	Group A, WMLs with gait disturbance	Group B, WMLs without gait disturbance	*p*
No. of patients	7 (3 men, 4 women)	7 (2 men, 5 women)	
Mean age (range), y	73.7 ± 4.6 (68–80)	77.3 ± 2.7 (72–80)	0.1
No. of lacunae in the striatum	1.14 ± 0.90	0.57 ± 0.54	0.17
Area of lacunae in the striatum (mm^2)	42.8 ± 30.3	21.7 ± 21.5	0.16
Motor UPDRS (0–108)	45.4 ± 15.0	8.2 ± 9.2	<0.001
MMSE score (0–30)	21.0 ± 6.3	27.0 ± 3.9	0.05
Dysarthria, No. (%)	3 (43)	0 (0)	0.19
Pseudobulbar palsy, No. (%)	1 (14)	0 (0)	>0.99
Urinary incontinence, No. (%)	3 (43)	1 (20)	0.56
Hypertension, No. (%)	5 (71)	4 (57)	>0.99
BP control (systolic BP >140 mmHg), No. (%)	1 (14)	0 (0)	>0.99
Diabetes mellitus, No. (%)	2 (29)	0 (0)	0.46
Cigarette smoking, No. (%)	3 (43)	3 (43)	>0.99
Microalbuminuria, No. (%)	2 (29)	0 (0)	0.46
Previous cerebrovascular events, No. (%)	2 (29)	1 (14)	>0.99
Previous myocardial infarction, No. (%)	2 (29)	1 (14)	0.47
Use of antiplatelets, No. (%)	5 (71)	5 (71)	>0.99
Use of anticoagulants, No. (%)	0 (0)	2 (29)	0.46
Total cholesterol, mg/dl	223.7 ± 23.8	199.7 ± 15.3	0.27
Triglyceride, mg/dl	106.2 ± 56.1	124.0 ± 54.0	0.55
Hematocrit, %	38.1 ± 2.6	35.9 ± 2.7	0.14

Data are presented as mean ± SD. *UPDRS* Unified Parkinson's disease rating scale; *MMSE* mini-mental state examination; *BP* blood pressure.

of our facility. If a subject was not fully competent due to dementia, we obtained full informed consent from his/her proxy. None of our patients had apparent lesions in the cerebral cortex, midbrain, or hippocampus. MR angiography or duplex color-coded sonography revealed an absence of apparent stenosis (greater than 50%) in the major intracranial and extracranial vessels. None of our patients had a history of taking any sedative-hypnotic benzodiazepines within the past 3 months that could have affected their BZR assessment. All subjects underwent a general physical and neurological examination, the motor subscale ratings of the Unified Parkinson's Disease Rating Scale (UPDRS), and Mini-Mental State Examination (MMSE) in a blind fashion with respect to the MRI results. We diagnosed VaP if the patient with WMLs met all the following criteria: symmetric parkinsonian syndrome; presence of gait disorder (including wide-based, small steppage, or frozen gait) plus at least one of the following two extrapyramidal signs: rigidity and bradykinesia; exclusion of drug-induced parkinsonism; poor response to adequate dose of anti-parkinsonian agents.

Synthesis of [^{11}C]FMZ, PET scanning, and data analysis

[^{11}C] FMZ was synthesized as previously described (Magata et al., 2003). Its radiochemical purity was found to be >98.5% and its specific activity was 53.4 ± 14.7 GBq/μmol ($n = 14$).

All 14 patients were scanned with a PET scanner (Advance; General Electric, Milwaukee, MI) that was run in 2-dimensional mode (Magata et al., 2003). Arterial blood samples were drawn, and metabolite correction of [^{11}C] FMZ was performed by the plasma extraction method (Magata et al., 2003) for 12 patients and by the whole blood extraction method, which was shown to be equivalent to the plasma extraction method (Magata et al., 2003), for 2 patients. Dynamic imaging was performed using 2D acquisition mode for 50 min after injection (sequence; 6 × 30 sec, 7 × 1 min, 5 × 2 min, 6 × 5 min). Six patients with parkinsonism and five patients without parkinsonism underwent ^{15}O gas steady-state examination within two weeks of FMZ-PET to quantify their CBF and $CMRO_2$ using the above PET scanner (Ihara et al., 2004). We followed the protocol for inhalation of [^{15}O] CO_2, [^{15}O] O_2, and [^{15}O] CO as previously reported (Yamauchi et al., 1999). PET data were reconstructed into 3-dimensional images parallel to the orbitomeatal line, so that each image consisted of 64 planes with 2-mm cubic voxels. Images were displayed using PMOD software version 2.4 (PMOD Technologies Ltd., Zurich, Switzerland) (Mikolajczyk et al., 1998).

ROI-based analysis

Regions of interest (ROIs) were defined on summed FMZ uptake images by point-and-click or manual drawing mode using PMOD (Mikolajczyk et al., 1998; Ihara et al., 2004). Briefly, for cortical regions, ROIs were drawn by hand in narrow strips that overlay the cortical mantle in the following regions: frontal cortex including Brodmann area's 8, 9, 10, 44, 45 and 46, temporal cortex including areas 21, 22 and 37, parietal cortex including areas 5, 7, 39 and 40, and occipital cortex including areas 17, 18 and 19, while intracranial sulci were avoided in order to minimize the partial volume effect. We also defined ROIs in the thalamus, basal ganglia (caudatoputamen), cerebellum, and centrum semiovale. Each patient's ROIs were saved. Based on a two compartment two parameter model using metabolite-corrected arterial input and PET-measured cerebral radioactivity, the distribution volume of FMZ ($FMZ\text{-}V_d$) was calculated in the defined ROIs by non-linear curve fitting based on the Gauss-Newton method. Values in homologous regions of each hemisphere were averaged. The CO, O_2, CO_2 images were coregistered to the FMZ image (Pmod software). The ROIs drawn on the FMZ image were transferred to the gas images, and their raw radioactivity counts were measured in all ROIs. Based on the steady-state method, regional CBF, $CMRO_2$ and OEF were calculated using each ROI value (Frackowiak et al., 1980). The $CMRO_2$ and OEF were corrected for CBV (Lammertsma and Jones, 1983).

Voxel-by-voxel analysis

Using PMOD, pixel-wise calculation was performed to yield parametric images of $FMZ\text{-}V_d$ (Mikolajczyk et al., 1998; Ihara et al., 2004). Briefly, the loaded image data were first pre-processed with arterial input curve. Classic Logan plot model was then applied to the time vector in each individual pixel. The pixel-wise results were assembled into parametric images of $FMZ\text{-}V_d$. These parametric images were analyzed using SPM2 (Wellcome Department of Cognitive Neurology, London, UK) that was run on Matlab6.5 (The MathWorks, Natick, MA). The images were transformed into the standard SPM2 PET template using the early phase of the FMZ image added (0–10 min) as a blood flow image. As a final pre-processing step, the images were smoothed using a 10 mm (full width at half maximum) isotropic Gaussian kernel.

Magnetic resonance imaging

Brain MRIs were obtained using a 1.5 Tesla MR scanner (Signa Horizon; General Electric). T1-weighted axial images were obtained using a spin

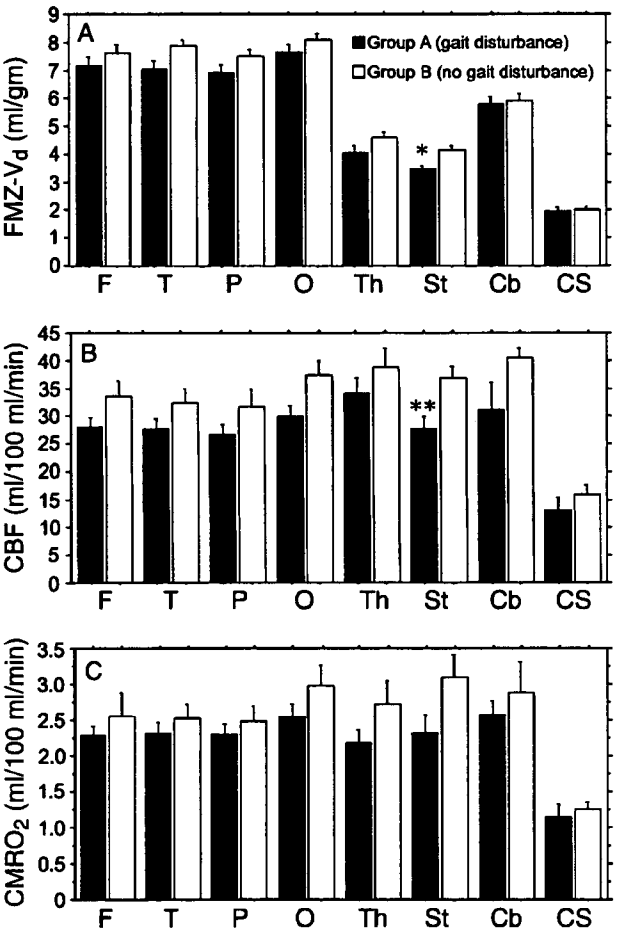

Fig. 2. Comparisons of $FMZ\text{-}V_d$ (**A**), CBF (**B**), and $CMRO_2$ (**C**) in the ROIs between patients with gait disturbance (Group A; solid bars) and those without gait disturbance (Group B; open bars). Bars represent SEM. *F* indicates frontal cortex; *T*, temporal cortex; *P*, parietal cortex; *O*, occipital cortex; *Th*, thalamus; *St*, striatum; *Cb*, cerebellum; and *CS*, centrum semiovale. $^{*}p < 0.001$; $^{**}p < 0.05$

echo pulse sequence with a repetition time of 400 msec and an echo time of 15 msec. Axial T2-weighted images were also obtained (repetition time, 3000 msec; echo time, 100 msec). Axial images were obtained in parallel to the orbitomeatal line. Slice thickness was 5 mm, with an interslice gap of 1.8 mm in the axial plane.

Lacunar infarction was defined as a hyperintensity area (5 mm ≤ diameter < 15 mm) on T2-weighted images which was seen as a low-signal intensity on T1-weighted images (Braffman et al., 1988). To reduce the risk of inclusion of enlarged perivascular spaces, lesions <5 mm were not counted as infarctions. The area of striatal lacunar infarction was approximated on a T2-weighted axial slice traversing the anterior horn of the ventricle and the thalamus (see Fig. 5) on a Macintosh PowerPC computer using the public domain NIH Image1.61 program (NIH).

The extent of cerebral atrophy was assessed by regional volumetric measures normalized for total intracranial area on three T2-weighted axial slices (see Fig. 5) using the NIH Image1.61 program. In brief, we outlined the inner boundary of the calvarium manually on T2-weighted axial images to determine the total intracranial area. The images were then binarized with intensity threshold set at 60% of mean intracranial pixel values within the outlined area. After the ventricular and subdural areas were semiautomatically outlined using the wand tool, the number of pixels in each area was divided by that in the total intracranial area to calculate normalized ventricular and subdural area. Finally, subtraction of the normalized ventricular and subdural areas from the total intracranial area (value 1.0) yielded normalized parenchymal area.

Statistical analysis

The statistical significance of intergroup differences was assessed with the Fisher's exact test for categorical variables, the Mann–Whitney *U*-test for continuous parametric variables of demographic data, and by ANOVA or ANCOVA for ROI-based analysis of FMZ-V_d, CBF, $CMRO_2$, and OEF (StatView5.0; SAS Institute, Cary, NC). Pearson correlation analysis was performed to observe possible links between the variables.

For voxel-based analysis, significant differences in FMZ-V_d between groups were estimated according to the general linear model at each and every voxel of the normalized and smoothed images (Friston et al., 1995). A linear contrast was used to test hypotheses relating to specific focal effects. The resulting set of voxel values for each contrast constituted a statistical parametric map (SPM{t}). The SPM{t} was thresholded at $P_{uncorr} < 0.001$ without multiple comparison.

Results

The demographic features of our patients were summarized in Table 1. The subjects were divided into two groups; i.e., patients with gait disturbance (so-called 'lower body' parkinsonism) suggestive of VaP (group A; $n = 7$) and those without it (group B; $n = 7$). Family history with regard to parkinsonism was unremarkable in all patients and there were no significant differences in patient age between groups ($p = 0.10$). The motor disability was measured by the motor UPDRS score; patients in group A showed significantly more severe motor disability than those in group B ($p < 0.001$). The MMSE score was reduced in the group A but with no statistical significance ($p = 0.053$).

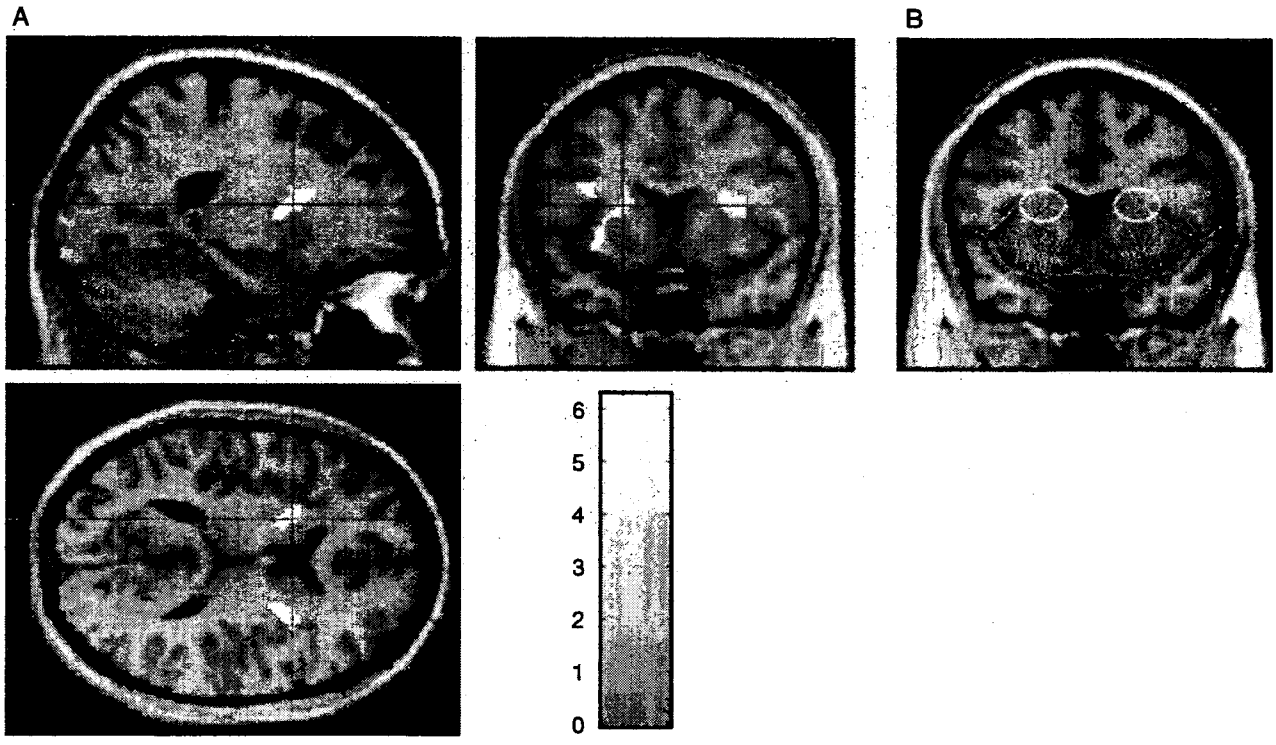

Fig. 3. Voxel-based analysis of [^{11}C]flumazenil-PET. A Statistical results were overlaid onto the brain slices of the standard MRI template of SPM2. Color scale: *t* scores (maximum $t = 6.83$, corresponding to $Z = 4.08$). *R* indicates right. B A diagram showing that FMZ-V_d is reduced in a part of the territory of lateral lenticulostriate arteries (artery, red lines; territory, dotted circles)

All patients had at least one risk factor for ischemic cerebrovascular disease which included hypertension, diabetes mellitus, hyperlipidemia, and smoking. Although there were no intergroup differences for these categorical variables, neurological deficits were found more frequently in the group A. Dysarthria and pseudobulbar palsy were found exclusively in the group A; these symptoms did not respond to adequate anti-parkinsonian drug treatment, supporting the diagnosis of VaP.

T2-weighted MRI revealed WMLs as well as pontine leukoaraiosis in all patients, while subcortical U fibers were consistently spared (Fig. 1). The mean ± SD number of lacunar infarctions in the striatum was slightly greater in the group A compared with the group B (Table 1: group A, 1.14 ± 0.90; group B, 0.57 ± 0.54; $p = 0.17$). Similarly, the area of lacunae in the striatum was larger in the group A (Table 1; group A, 42.8 ± 30.3 mm^2; group B, 21.7 ± 21.5 mm^2; $p = 0.16$). Consistent with such anatomical changes, FMZ-V_d imaging showed lower values of striatal FMZ-V_d in the group A (Fig. 1).

ROI-based analysis demonstrated that FMZ-V_d tended to be lower in the group A than in the group B (Fig. 2A).

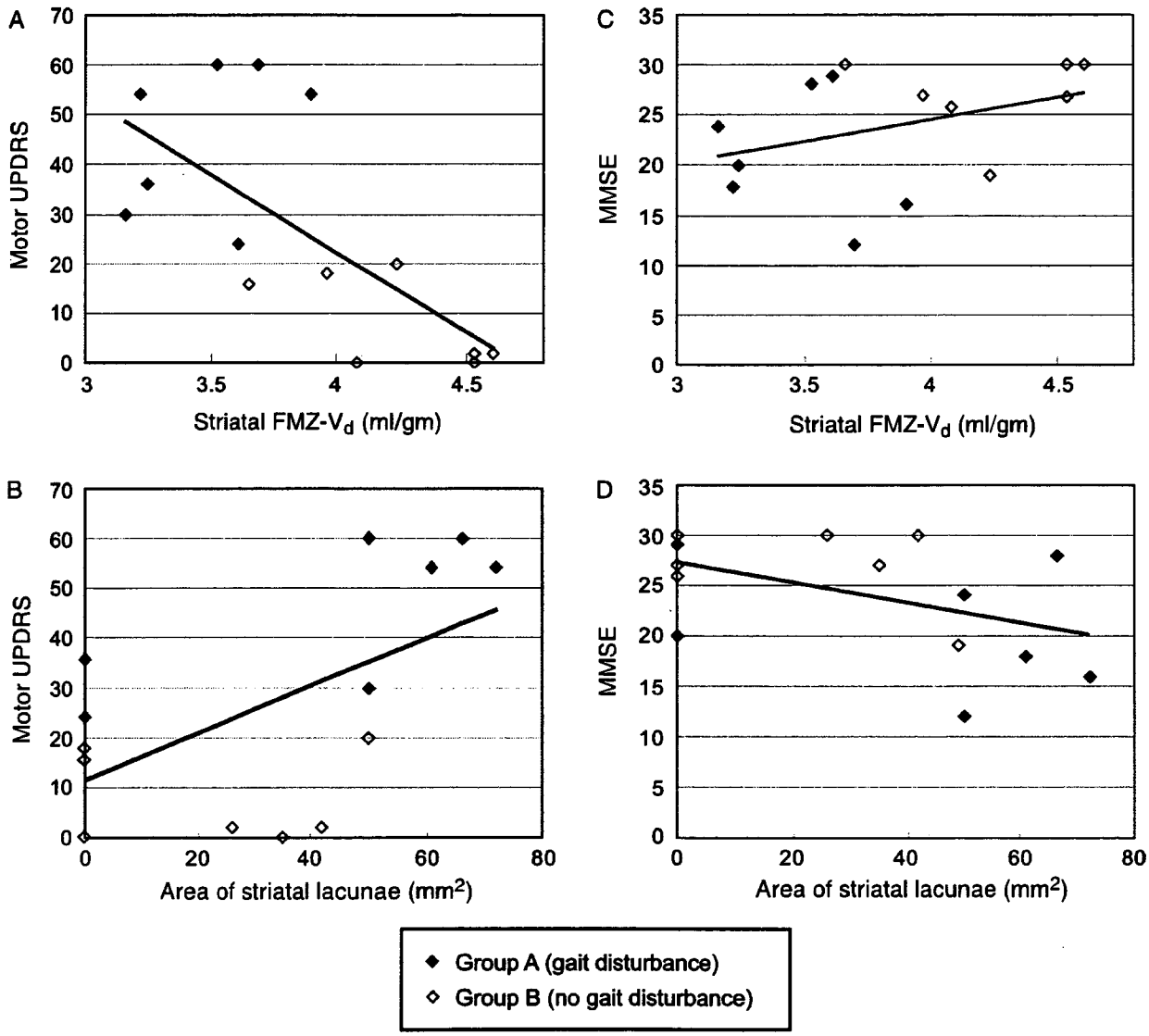

Fig. 4. Correlation of motor UPDRS scores with FMZ-V_d values and infarcted areas in the striatum. (**A**, **B**) The motor UPDRS scores were significantly correlated with the striatal FMZ-V_d values (**A**; r (Pearson) = 0.70; $p < 0.005$) or the striatal infarcted areas (**B**; $r = 0.57$; $p = 0.03$). (**C**, **D**) The MMSE scores were not significantly correlated with the striatal FMZ-V_d values (**C**; $r = 0.35$; $p = 0.21$) or the striatal infarcted areas (**D**; $r = 0.48$; $p = 0.09$). Closed square, patients with gait disturbance (Group A; $n = 7$); open square, patients without gait disturbance (Group B; $n = 7$)

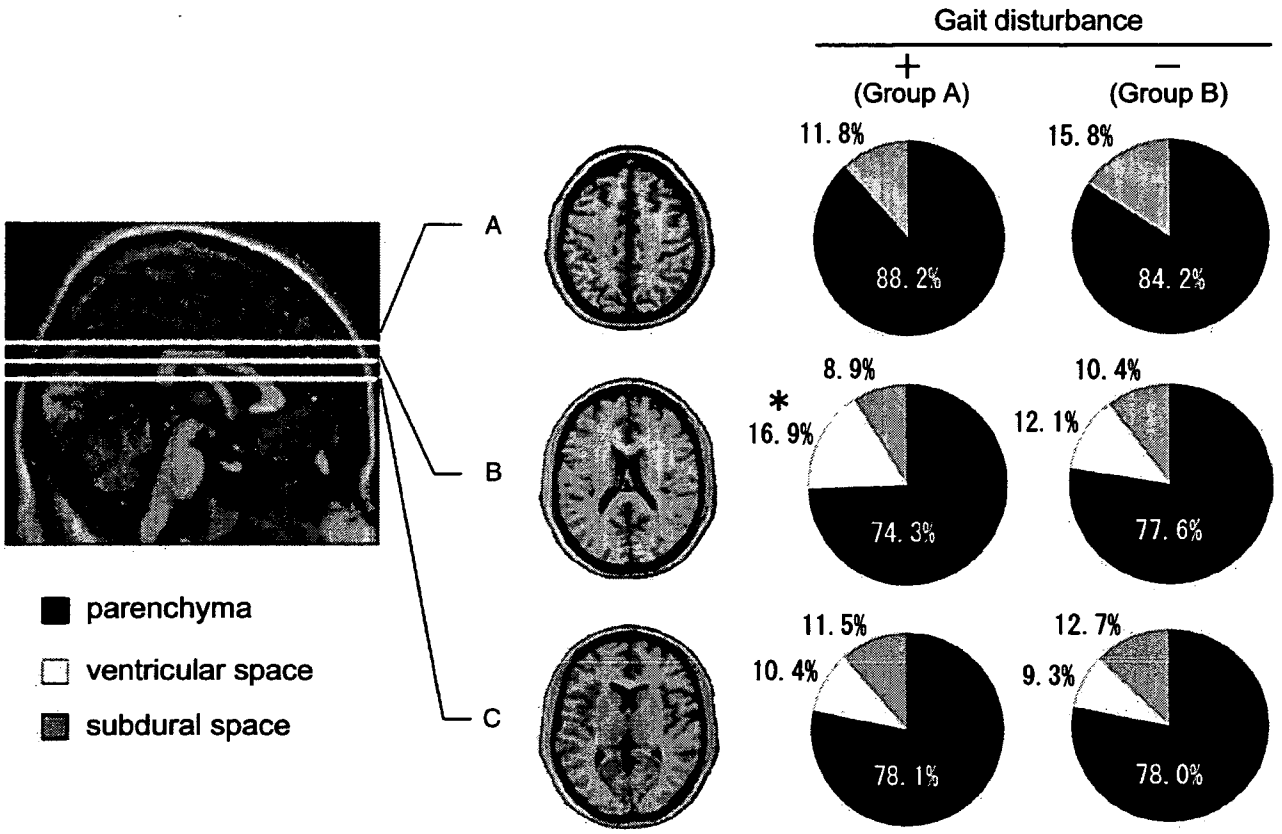

Fig. 5. Comparison of the regional brain volumetry between patients with and without gait disturbance. Brain atrophy was assessed on the three axial slices; immediately superior to the ventricle (A), through the body of the ventricle (B), and through the anterior and posterior ventricular horns (C). Regions occupied by brain parenchyma, subdural space, and ventricular space are indicated as the ratio to total intracranial area at each level. $^{**}p<0.05$

These reductions reached significance in the striatum (17.8%; $p<0.001$), although no significant difference was found in the other areas. The significant difference in the striatal FMZ-V_d still held true after adjusting for differences in MMSE scores by ANCOVA analysis ($p=0.002$). CBF was also reduced in the group A (Fig. 2B), although this reduction only reached significance in the striatum (25.4%; $p<0.05$). $CMRO_2$ also tended to be lower in group A, but these values did not reach statistical significance (Fig. 2C). The largest reduction in $CMRO_2$ was detected in the striatum (25.3%, $p=0.076$). No significant differences were detected in OEF.

SPM analysis showed that FMZ-V_d was significantly reduced in the dorsal striatum bilaterally in the group A ($P_{uncorr}<0.001$; Fig. 3A). The area of reduced FMZ-V_d corresponded to a part of the territory supplied by lateral lenticulostriate arteries (Fig. 3B).

Given the significant reduction of striatal FMZ-V_d in group A patients, we next investigated a possible correlation between striatal FMZ-V_d and parkisonian motor handicap assessed by motor UPDRS. We found a significant inverse correlation of striatal FMZ-V_d with motor UPDRS score (Fig. 4A; $r=0.70$, $p<0.005$). In addition, the area of striatal lacunae positively correlated with the motor UPDRS score (Fig. 4B; $r=0.57$, $p<0.05$); however, the correlation was weaker than that between striatal FMZ-V_d and the motor UPDRS score. The MMSE scores were not significantly correlated with the striatal FMZ-V_d (Fig. 4C; $r=0.035$, $p=0.21$) or with the areas of striatal lacunae (Fig. 4D; $r=0.48$, $p=0.09$).

The regional volumetry showed a significant difference in the area of ventricular bodies, but not in the area of ventricular horns between the groups A and B (Fig. 5).

Discussion

The above results showed that FMZ-V_d and CBF were significantly reduced in the striatum of patients with WMLs who manifested gait disturbance ('lower body' parkinsonism) compared to those who did not. Since FMZ binding reflects neuronal integrity (Heiss et al., 1998; Ihara et al., 2001, 2004) and is relatively unaffected by CBF (Holthoff

et al., 1991), our results suggest that patients with WMLs develop Parkinson-like gait disorders probably due to impaired neuronal integrity in the striatum resulting from ischemia. Consistent with this was the increased number of lacunae in the striatum in our patients with Parkinson-like gait disorders and a previous ^{15}O PET study suggesting that small vessel pathology leads to local ischemic changes in the striatum along with WMLs, jointly contributing to VaP (De Reuck et al., 2001). The lateral lenticulostriate arteries mainly supply the striatum including the putamen (Braffman et al., 1988), and reduced blood flow within several lenticulostriate arteries might impair striatal integrity insidiously. If such striatal flow reduction exceeds a certain threshold and/or spreads to become bilateral, VaP may eventually occur. Given that the striatum plays a pivotal role in correlating the basal ganglia-thalamocortical motor system (higher-order motor control) to the nigrostriatal dopaminergic system (extrapyramidal motor control) (Thompson and Marsden, 1987), chronic ischemic damage to the striatum may well contribute to developing motor impairment such as VaP.

In addition to the 'direct' striatal ischemia, a global loss of neuronal connections may also have affected the neuronal integrity in the striatum because a significant reduction of striatal FMZ-V_d can be interpreted as a group effect across all brain regions. In fact, the ROI-based analysis showed global reductions in FMZ-V_d, rCBF, and $rCMRO_2$ in group A (gait disturbance) patients. Furthermore, the body of the ventricle was significantly dilated in the group A patients, indicative of atrophy and damage of the deep white matter. In such damaged white matter, motor circuits between cortical and subcortical structures, including the basal ganglia-thalamocortical circuit, may be subject to retrograde and/or transsynaptic neuronal degeneration, secondarily disrupting neuronal integrity in the striatum (Brodal, 1981). As is suggested by a previous CT analysis (van Zagten et al., 1998), ischemic damage to the striatum as well as the deep white matter could synergistically disrupt the cortico-subcortical motor circuits, thus contributing to the development of VaP.

To reinforce our interpretation of the results, we should exclude the possibility that the presence of dementia in the group A patients confounded the results because the VaP and vascular dementia are related entities and the mean MMSE score was reduced to 21 points in the group A patients, which is below the cut-off points for dementia. The global reductions in FMZ-V_d, rCBF, and $rCMRO_2$ in group A patients may represent a basis for the reduced MMSE scores. However, the MMSE scores did not correlate with the striatal FMZ-V_d values, and adjustment for differences in MMSE scores did not eliminate the significant difference in the striatal FMZ-V_d between group A and B patients. Furthermore, we found a significant correlation of the motor UPDRS scores with the infarcted areas in the striatum, and more strongly, with the FMZ-V_d values in the striatum. Hence, we conclude that the anatomical as well as functional alterations in the striatum are associated with Parkinson-like gait disorders but not with dementia in patients with WMLs.

In other movement disorders including IPD and progressive supranuclear palsy, the number of striatal BZRs was reported to be within normal limits in postmortem brains using [^{3}H]flunitrazepam *ex vivo* autoradiography (Maloteaux et al., 1998). In addition, FMZ-PET examination in patients with progressive supranuclear palsy and multiple system atrophy demonstrated preservation of BZRs in the striatum (Gilman et al., 1994; Foster et al., 2000). These findings suggest that striatal neuronal integrity is more severely impaired in VaP compared to other movement disorders. The high vulnerability of the striatum in small vessel disease may partially explain the difference (Pantoni et al., 2002).

Certain clarifications need to be addressed regarding the accuracy of the FMZ-V_d. Since the striatal density of BZRs is relatively low, the striatum was reported to exhibit a high variance in B_{max} and K_d values when obtained from FMZ-PET (Abadie et al., 1992). In our study, however, we placed the striatal ROI on the summed FMZ uptake images, and utilized the differences in FMZ uptake among the striatum, the cerebral cortex, and the ventricle. The SEM values were not large in the striatum (see Fig. 2), implying that the determinations of ROIs in the striatum were reliable. Second, significant atrophy could lead to displacement of the striatum and affect our SPM analysis. However, on the axial slice through the striatum and ventricular horns, regions occupied by brain parenchyma, subdural space, and ventricular space were comparable between the two cohorts, thus making unlikely the possibility of striatal displacement. The consistent results between the ROI-based analysis and the SPM analysis further support the accuracy of FMZ-V_d in the striatum.

In conclusion, differences in neuronal integrity in the striatum may determine whether patients with WMLs develop VaP or not. Although the relatively small number of subjects and the absence of neuropathological confirmation are potential limits of this study, the strong correlation between the striatal FMZ-V_d values and the UPDRS scores supports the above conclusion. Thus, the striatal FMZ binding could be a reliable diagnostic marker for VaP. Since therapeutic intervention could be effective in preventing the latent progression of VaP symptoms (Zijlmans et al.,

1995; Winikates and Jankovic, 1999; Foltynie et al., 2002; Sibon et al., 2004), further research is warranted as to how the functional integrity of the striatum can be maintained.

Acknowledgments

This study was supported by a Grant-in-Aid for Japan Society for the Promotion of Science (JSPS) Fellows (M.I.), and also partly supported by Grant-in-Aid for Scientific Research on Priority Areas (B) from JSPS and "Science of Mind" from the Japanese Ministry of Health and Labor (H.F.).

References

Abadie P, Baron JC, Bisserbe JC, Boulenger JP, Rioux P, Travere JM, Barre L, Petit-Taboue MC, Zarifian E (1992) Central benzodiazepine receptors in human brain: estimation of regional Bmax and KD values with positron emission tomography. Eur J Pharmacol 213: 107–115

Bhatia KP, Marsden CD (1994) The behavioural and motor consequences of focal lesions of the basal ganglia in man. Brain 117: 859–876

Braffman BH, Zimmerman RA, Trojanowski JQ, Gonatas NK, Hickey WF, Schlaepfer WW (1988) Brain MR: pathologic correlation with gross and histopathology, 1: lacunar infarction and Virchow Robin spaces. AJR Am J Roentgenol 9: 621–628

Brodal A (1981) Neurological anatomy in relation to clinical medicine, 3rd edn. Oxford University Press, New York

De Reuck J, Siau B, Decoo D, Santens P, Crevits L, Strijckmans K, Lemahieu I (2001) Parkinsonism in patients with vascular dementia: clinical, computed- and positron emission-tomographic findings. Cerebrovasc Dis 11: 51–58

Ebersbach G, Poewe W (2006) Vascular parkinsonian syndrome. Nervenarzt 77: 139–144, 146–147

Foltynie T, Barker R, Brayne C (2002) Vascular parkinsonism: a review of the precision and frequency of the diagnosis. Neuroepidemiology 21: 1–7

Foster NL, Minoshima S, Johanns J, Little R, Heumann ML, Kuhl DE, Gilman S (2000) PET measures of benzodiazepine receptors in progressive supranuclear palsy. Neurology 54: 1768–1773

Frackowiak RS, Lenzi GL, Jones T, Heather JD (1980) Quantitative measurement of regional cerebral blood flow and oxygen metabolism in man using ^{15}O and positron emission tomography: theory, procedure, and normal values. J Comput Assist Tomogr 4: 727–736

Friston KJ, Holmes AP, Worsley KJ, Poline JP, Frith CD, Frackowiak RSJ (1995) Statistical parametric maps in functional imaging: a general linear approach. Hum Brain Mapp 2: 189–210

Gilman S, Koeppe RA, Junck L, Kluin KJ, Lohman M, St Laurent RT (1994) Patterns of cerebral glucose metabolism detected with positron emission tomography differ in multiple system atrophy and olivopontocerebellar atrophy. Ann Neurol 36: 166–175

Heiss WD, Grond M, Thiel A, Ghaemi M, Sobesky J, Rudolf J, Bauer B, Wienhard K (1998) Permanent cortical damage detected by flumazenil positron emission tomography in acute stroke. Stroke 29: 454–461

Holthoff VA, Koeppe RA, Frey KA, Paradise AH, Kuhl DE (1991) Differentiation of radioligand delivery and binding in the brain: validation of a two-compartment model for [^{11}C]flumazenil. J Cereb Blood Flow Metab 11: 745–752

Ihara M, Fukuyama H, Lee T, Takao S, Kohara N, Shibasaki H (2001) Delayed synaptic dysfunction of association cortices in carbon monoxide intoxication. Ann Neurol 50: 829–830

Ihara M, Tomimoto H, Ishizu K, Mukai T, Yoshida H, Sawamoto N, Inoue M, Doi T, Hashikawa K, Konishi J, Shibasaki H, Fukuyama H (2004) Decrease in cortical benzodiazepine receptors in symptomatic patients with leukoaraiosis. a positron emission tomography study. Stroke 35: 942–947

Jellinger KA (2003) How valid is the clinical diagnosis of Parkinson's disease in the community? J Neurol Neurosurg Psychiatry 74: 1005–1006

Lammertsma AA, Jones T (1983) Correction for the presence of intravascular oxygen-15 in the steady-state technique for measuring regional oxygen extraction ratio in the brain: 1. Description of the method. J Cereb Blood Flow Metab 3: 416–424

Magata Y, Mukai T, Ihara M, Nishizawa S, Kitano H, Ishizu K, Saji H, Konishi J (2003) Simple analytical method of ^{11}C-flumazenil metabolite in blood. J Nucl Med 44: 417–421

Maloteaux JM, Luabeya MA, Vanisberg MA, Laterre EC, Laduron PM, Javoy-Agid F, Agid Y (1998) Benzodiazepine receptors in normal human brain, in Parkinson's disease and in progressive supranuclear palsy. Brain Res 446: 321–332

Mikolajczyk K, Szabatin M, Rudnicki P, Grodzki M, Burger C (1998) A JAVA environment for medical image data analysis: initial application for brain PET quantitation. Med Inform (Lond) 23: 207–214

Olsen RW (1981) The GABA postsynaptic membrane receptor-ionophore complex. Site of action of convulsant and anticonvulsant drugs. Mol Cell Biochem 39: 261–279

Pantoni L, Palumbo V, Sarti C (2002) Pathological lesions in vascular dementia. Ann N Y Acad Sci 977: 279–291

Rampello L, Alvano A, Battaglia G, Raffaele R, Vecchio I, Malaguarnera M (2005) Different clinical and evolutional patterns in late idiopathic and vascular parkinsonism. J Neurol 252: 1045–1049

Schmidt R, Hayn M, Fazekas F, Kapeller P, Esterbauer H (1996) Magnetic resonance imaging white matter hyperintensities in clinically normal elderly individuals. Correlations with plasma concentrations of naturally occurring antioxidants. Stroke 27: 2043–2047

Sibon I, Fenelon G, Quinn NP, Tison F (2004) Vascular parkinsonism. J Neurol 251: 513–524

Thompson PD, Marsden CD (1987) Gait disorder of subcortical arteriosclerotic encephalopathy: Binswanger's disease. Mov Disord 2: 1–8

van Zagten M, Lodder J, Kessels F (1998) Gait disorder and parkinsonian signs in patients with stroke related to small deep infarcts and white matter lesions. Mov Disord 13: 89–95

Winikates J, Jankovic J (1999) Clinical correlates of vascular parkinsonism. Arch Neurol 56: 98–102

Yamanouchi H, Nagura H (1997) Neurological signs and frontal white matter lesions in vascular parkinsonism. A clinicopathologic study. Stroke 28: 965–969

Yamauchi H, Fukuyama H, Nagahama Y, Nishizawa S, Konishi J (1999) Uncoupling of oxygen and glucose metabolism in persistent crossed cerebellar diaschisis. Stroke 30: 1424–1428

Zijlmans JC, Thijssen HO, Vogels OJ, Kremer HP, Poels PJ, Schoonderwaldt HC, Merx JL, van 't Hof MA, Thien T, Horstink MW (1995) MRI in patients suspected of vascular parkinsonism. Neurology 45: 2183–2188

European Journal of Neurology 2007, 14: 95–101 doi:10.1111/j.1468-1331.2006.01567.x

Subinsular vascular lesions: an analysis of 119 consecutive autopsied brains

H. Tomimoto[a], J. Lin[a], M. Ihara[a], R. Ohtani[a], A. Matsuo[a] and Y. Miki[b]
Departments of [a]Neurology and [b]Diagnostic Radiology, Graduate School of Medicine, Kyoto University, Sakyo-ku, Kyoto, Japan

Keywords:
autopsied brain, cerebrovascular disease, dementia, insula, white matter,

Received 12 January 2006
Accepted 3 May 2006

The insula of Reil constitutes a functionally intriguing complex of the brain related to multifunctional activities. We examined the subinsular region in 119 consecutively autopsied patients, as T2 hyperintense lesions are frequently observed in magnetic resonance diagnosis of this region. The patients were admitted in neurology wards and were diagnosed as having cerebrovascular disease in 55 patients (46%), other neurological diseases in 57 patients (48%) and non-neurological diseases in seven patients (6%). Demyelination of the white matter was semi-quantified as a fiber density score (percent stained area/total area) with computer-assisted image analysis on Klüver–Barrera-stained sections. Astrogliosis was assessed by immunohistochemistry for glial fibrillary acidic protein. The lesion analysis showed a dilated perivascular space in 29 patients (24%), demyelination (fiber density score less than the mean − 1 SD) in 27 patients (23%), slit-shaped lesion in six patients (5%), lacunar infarction in one patient (1%) and cerebral hemorrhage in one patient (1%). A histologic–radiologic comparison in two patients with subcortical ischemic vascular dementia showed correspondence between subinsular hyperintensities, and demyelination, gliosis and a dilated perivascular space. These results indicate that subinsular lesions rarely signifies focal vascular lesions, and are consisted of demyelination, gliosis and a dilated perivascular space.

Introduction

The insula of Reil is located beneath the frontoparietal and temporal opercula, and covers the basal ganglia, the external capsule, the claustrum and the capsula extrema. It has a diverse connection with the entire cerebral cortex, especially frontoparietal and temporal cortices, the basal ganglia, thalamus and the limbic structures. Therefore, it constitutes a functionally intriguing complex related to multifunctional activities of the brain. These include a pain processing in the human secondary somatosensory area (SII), visceral motor sensory processing and gustatory, vestibular and neuropsychiatric functions. Herein, we use the term of 'subinsular region' to refer to the insular cortex, extreme capsule, claustrum and the external capsule. This region also harbors trajectories passing through it, which include uncinate fasciculus [1], inferior occipitofrontal fasciculus, Meyer's loop [1] and cholinergic projection fibers to the cerebral cortices [2]. This cholinergic projection fibers may be impaired strategically by subinsular lesions in patients with subcortical ischemic vascular dementia (SIVD) [3–5] and cerebral autosomal dominant arteriopathy with subcortical infarcts and leukoencephalopathy (CADASIL) [6].

The subinsular region is vulnerable to ischemic damages, as it is located in the blood flow cliff between the supply from the lateral lenticulostriate arteries and the insular arteries arising from the M3 segment of the middle cerebral artery [7,8]. Therefore, WM lesions in the subinsular region are believed to be ischemic in nature, and continuum of the periventricular WM lesions in the frontal horn. However, little information is available on the neuropathologic substrates corresponding to subinsular hyperintense lesions found on T2-weighted magnetic resonance (MR) images. In CADASIL brains, the correspondents of these lesions are spongiosis and subcortical lacunar lesions in the anterior temporal pole [9], but remain elusive in the subinsular region. In a postmortem MR imaging study of epilepsy patients, Song et al. has addressed subinsular hyperintense lesions to be dilated perivascular spaces [10].

The purpose of the present study is twofold. First, we sought to determine the varieties and frequencies of pathological and non-pathological findings in the subinsular region, as this information can help to understand the nature of the subinsular hyperintense lesions on MR images. Secondly, we compared the premortem radiological findings against the postmortem pathological findings especially in SIVD, and directly determined the pathological nature of subinsular WM lesions, although

Correspondence: Hidekazu Tomimoto, MD, Department of Neurology, Graduate School of Medicine, Kyoto University, Sakyo-ku, Kyoto 606-8507, Japan (tel.: 81 75 751 3766; fax: 81 75 751 3766; e-mail: tomimoto@kuhp.kyoto-u.ac.jp).

premortem radiological films were available only in a limited number of patients.

Subjects and methods

Autopsy specimens

The diagnosis of each patient was based on the combination of pertinent clinical and laboratory findings, and an autopsy examination. We examined 119 brains, including seven from patients who did not have any neurological symptoms or brain lesions (non-neurological control group), 55 from patients with cerebrovascular disease (the CVD group) and 57 from patients with other neurological diseases (the OND group). These patients were autopsied from January 1993 to December 2001 in our institution and its affiliated hospitals which are treating community-dwelling population in the urban area of Kyoto Prefecture. Seven patients had both CVD and ONDs, and they were classified to the OND group. Out of the 119 patients, there were three patients with SIVD, in which clinical and radiologic findings met all of the clinical criteria proposed by Bennett et al. [11]. All patients had a record on radiologic information based on either of computed tomographic (CT) or MR images. Premortem films were available in six patients with CT, and three with MR images which included one with multiple lacunar infarctions and two with SIVD (No. 58 and 67). Hyperintensities were graded in MR images using the following 4-point scale as described by Fazekas et al. [12]: 0, no lesions present; 1, caps and pencil-thin lining; 2, smooth halo; and 3, irregular hyperintensities extending into the deep white matter. The hyperintensities in the external capsule were graded as 0 if they were absent; 1 if their length was shorter than one-fourth of the external capsule; 2, between one-fourth and a half; and 3, longer than one half. Radiological and neuropathological correlations were summarized in Table 1.

Immunohistochemistry

Standard histological examinations were performed on paraffin sections (6 μm-thick) with Klüver–Barrera staining for the observation of myelinated nerve fibers, and hematoxyline and eosin (H&E) staining. A mouse monoclonal antibody against glial fibrillary acidic protein (GFAP; Dakopatts, Glostrup, Denmark, 0.5 μg/ml) was used in the present study. After incubation with the primary antibody, the sections were treated with a biotinylated anti-mouse antibody (Vector Laboratories, ×200) and an avidin–biotin complex (Vector Laboratories, Burlingame, CA, USA, ×200) in 0.02 M PBS containing 0.3% Triton-X (PBST). The sections were finally incubated in 0.01% diaminobenzidine tetrahydrochloride and 0.005% H_2O_2 in 50 mM Tris–HCl (pH 7.6). To test the specificity of the immunohistochemical reaction, control sections were treated with normal mouse IgG instead of the primary antibody.

Image analysis

The subinsular region was defined as the insular cortex, extreme capsule, claustrum and the external capsule. The severity of demyelination in the external and extreme capsules was semi-quantified as follows. The positive areas above an intensity threshold (set at 60% of the mean pixel values within the outlined area of Klüver–Barrera staining) were digitized on an Apple personal computer (PC7500) with a LS-1000 film scanner (Nikon) at a resolution of 1350 dots per inch. These data were saved as 8-bit gray scale PICT files (256 shades of gray), and were analyzed using the NIH image analyzer program by counting the percentage of positive area as the score for myelinated fiber density (myelinated fiber density score). Each image measured 1060.6 × 757.6 μm and consisted of 1893 × 1197 pixels. The myelinated fiber density score was averaged across three representative rectangles from each of the regions of interest in each patient (Fig. 1; labels 1–3 for the external capsule and 4–6 for the extreme capsule). Subinsular demyelination was judged to be present if the fiber density score was less than the mean − 1 SD of all the fiber density scores in either the external or extreme capsules (39.4% for the former and 42.4% for the latter). In a preliminary experiment with eight brains, reproducibility of the estimation ranged at most a 4% variance [16].

Dilatation of the perivascular space was judged to be present if five to six or more small arteries had a perivascular space with a diameter 1.5 times larger than that of the small arteries. Lacunar infarction denoted a small cavity with a diameter between 3 and 15 mm.

Statistical analysis

The statistical significance of intergroup differences was assessed by a one-factor ANOVA followed by Scheffe's F procedure between each group, using StatView II software (version 5.0, for Macintosh; SAS Institute, Tokyo, Japan).

Results

Amongst the 119 patients, 55 were diagnosed with CVD (46%), 57 with ONDs (48%) and seven with non-neurological diseases (6%) (Table 2). The other neurological patients were consisted of 45 with neurodegenerative

Table 1 Radiological and pathological correlation in each patient

Patient no.	Age/gender	Disease	Radiological findings (Rt/Lt) APV	SI	Pathological findings (Rt/Lt SI) Demyelination	Dilated perivascular space
MRI						
58	86/F	SIVD	3/3	3/3	+/+	+/+
67	82/F	SIVD	3/3	2/3	+/+	+/+
114	54/M	Multiple lacunar infarction	2/2	1/1	-/-	-/-
CT						
28	72/F	Multiple lacunar infarction	+/+	0/0	-/-	-/-
38	84/F	SDAT	-/-	1/1	-/-	+/+
80	86/F	Multiple lacunar infarction	+/+	2/2	+/+	-/-
86	90/F	SDAT	+/+	2/1	+/+	+/+
94	88/F	SDAT	+/+	1/2	-/-	+/+
102	84/F	SDAT	-/-	2/3	+/+	+/+

APV, anterior periventricular region; Rt, right; Lt, left; SI, subinsular region; SIVD, subcortical ischemic vascular dementia; SDAT, senile dementia of Alzheimer type. The scores in the radiological findings were determined as described in the Subjects and methods.

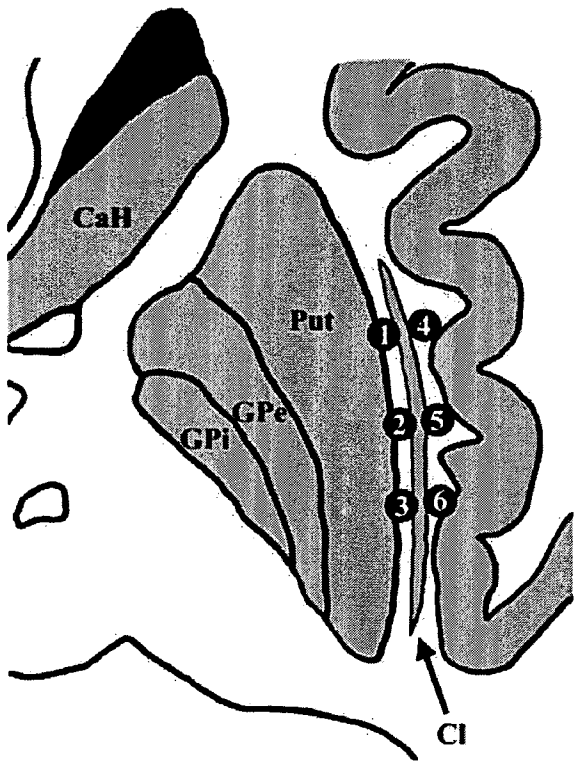

Figure 1 A schematic drawing indicating the region for semi-quantitative image analysis. The labels (1)–(3) indicate for the external capsule and (4)–(6) for the extreme capsule. CaH, caudate head; Put, putamen; GPe, external segment of the globus pallidus; GPi, internal segment of the globus pallidus; Cl, claustrum.

disorders, six with central nervous system infection, three with neuromyopathy, two with brain tumor and one with metabolic encephalopathy. The non-neurological disease patients were consisted of three with pulmonary cancer, one with hepatic cancer, two with pneumonia, and one with rheumatoid arthritis. The mean age in the CVD group was significantly higher than the OND and non-neurological groups. The brain weight was significantly lower in the CVD and OND groups than in the non-neurological control group. Amongst the confounding factors including age, brain weight and myelinated fiber density scores in the external and extreme capsules, a significant correlation was found only between the myelinated fiber density scores of the external and extreme capsules ($R = 0.868$). There were no significant differences in the myelinated fiber density scores between the three groups in both the external and extreme capsules (Table 2), nor any relationships to age ($R = 0.009$ for the external capsule; $R = 0.014$ for the extreme capsule). In the CVD group, however, the myelinated fiber density scores were significantly lower in patients with cerebral hemorrhage than small vessel infarction.

A dilated perivascular space was observed in 29 of 119 patients (24%), more frequently in the CVD and OND groups than in the non-neurological control group (Table 3). In these brains, small arteries with a dilated perivascular space penetrated into the insular cortex, and coursed medio-superiorly in the lower one-third of the extreme capsule (Fig. 2A). On the contrary, the lateral lenticulostriate arteries with a markedly

Table 2 Baseline characteristics and nerve fiber density scores in each group

	Number of patients (male)	Age (years)	Brain weight (g)	Nerve fiber density scores (%)	
				External capsule	Extreme capsule
CVD	55 (29)	77 ± 14*	1151 ± 131	48.6 ± 10.1	51.0 ± 9.3
Cerebral hemorrhage	7 (4)	79 ± 10	1146 ± 170	40.8 ± 11.1**	42.4 ± 11.1**
Small vessel infarction	27 (12)	79 ± 11	1157 ± 127	49.9 ± 9.3	52.9 ± 7.3
Cortical infarction	21 (13)	74 ± 17	1144 ± 132	49.6 ± 10.3	51.4 ± 9.9
OND	57 (30)	66 ± 11	1177 ± 209	48.9 ± 9.0	50.7 ± 8.2
Non-neurological controls	7 (4)	66 ± 11	1252 ± 129	50.8 ± 9.7	53.1 ± 6.9

CVD, cerebrovascular disease; OND, other neurological disease. Small vessel infarction comprises multiple lacunar infarctions and subcortical ischemic vascular dementia. *Significant at $P < 0.01$ compared with the other two groups. **Significant at $P < 0.05$ compared with the small vessel infarction.

Table 3 Types of lesions amongst the 119 consecutive autopsied brains

Type of lesions	*n* (%)
1. Dilated perivascular space	29 (24)
CVD	15/55
OND	13/57
Non-neurological controls	1/7
2. Demyelination	27 (23)
CVD	15/55
Cerebral hemorrhage	5
Multiple lacunar infarctions	4
SIVD	3
Cortical infarction	2
Hypoxic encephalopathy	1
OND	10/57
Non-neurological controls	2/7
3. Slit-shaped lesion in the lateral edge of the putamen	6 (5)
CVD	4/55
OND	1/57
Non-neurological controls	1/7
4. Lacunar infarction	1 (1)
5. Primary hemorrhage	1 (1)

CVD, cerebrovascular disease; OND, other neurological disease; SIVD, subcortical ischemic vascular dementia. The numbers in parenthesis indicate the percent ratio of the 119 brains. Demyelination was overlaid with a dilated perivascular space in nine brains and with the slit-shaped lesion in one brain.

dilated perivascular space occasionally penetrated into the lower lateral edge of the putamen (Fig. 2B). Subinsular demyelination, with a myelinated fiber density score less than the mean − 1 SD, was observed in 27 of the 119 patients (23%) (Fig. 2C,D). Twelve of the 27 patients were suffering from small vessel disease, including five with hypertensive cerebral hemorrhage, four with multiple lacunar infarctions and three with SIVD (Table 3). The immunohistochemistry for GFAP confirmed that subinsular demyelination was associated with astrogliosis (Fig. 2E,F). Slit-shaped lesions, being different from a lacunar infarction in their shapes, were observed in the lateral edge of the putamen in six patients, in which three suffered from hypoxic encephalopathy (Table 3, data not shown). The subinsular demyelination coexisted with a dilated perivascular space in nine patients, and with a slit-shaped lesion in one patient. Focal lesions were rarely found, only with one patient having a lacunar infarction restricted to the lower end of the extreme capsule and the insular cortex (Fig. 2G), and one patient having a subinsular hemorrhage (Fig. 2H).

A relatively good correlation was found between radiologic–histologic findings in the subinsular region (Table 1). With respect to MR images, linear hyperintense lesions were found in the subinsular region of the two SIVD patients (No. 58 and 67). Patient No. 58 had linear hyperintensities (Fig. 3A,B), whereas those in patient No. 67 were ribbon-like and limited to the anterior half of the subinsular region (Fig. 3C,D). Demyelination in the external capsule was obvious in patient No. 58 when compared with the control patients (Fig. 3E,F), with myelinated fiber density scores of 33.9% for the external capsule. In contrast, patient No. 67 had mild demyelination (Fig. 3G), with myelinated fiber density scores of 37.9% in the external capsule, and had a dilated perivascular space in the subinsular region at the lower putamen level (Fig. 3H). Neither of these two patients had focal lesions such as lacunar infarction or cerebral hemorrhage in the subinsular region.

Discussion

White matter lesions in the external capsules are known to be frequently observed in radiological diagnosis for CADASIL and SIVD [9,13–16]. The present study further revealed that subinsular WM lesions correspond pathologically to demyelination and gliosis at the mid-putamen level, and a dilated perivascular space at the lower putamen level in SIVD. These neuropathological substrates for WM lesions were observed not only in the CVD group but also in

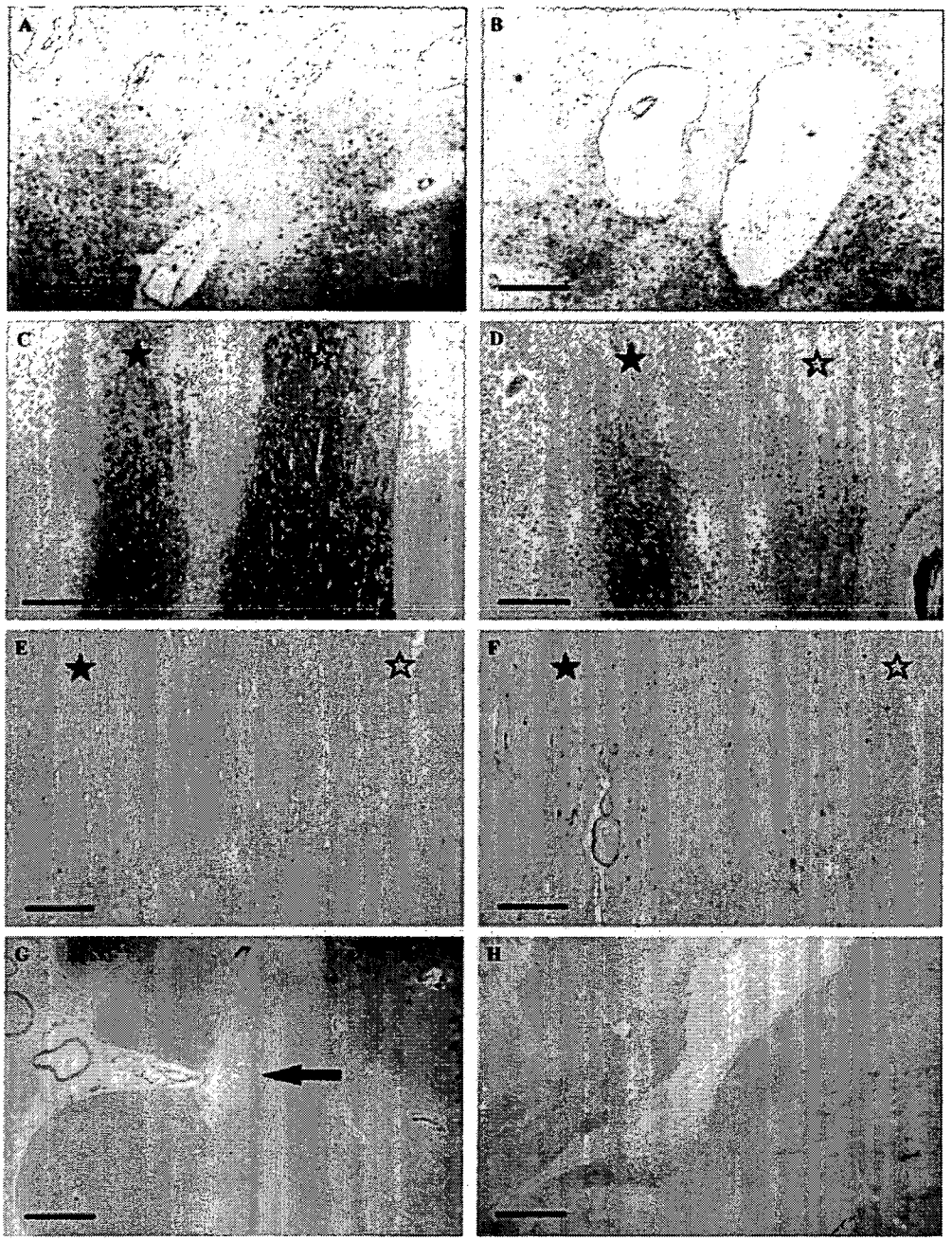

Figure 2 Photomicrographs of the H&E staining (A, B, G, H), Klüver–Barrera staining (C, D) and immunohistochemistry for GFAP (E, F). A dilated perivascular space in the lower one-third of the extreme capsule (A); a lateral lenticulostriate artery with a dilated perivascular space turns dorsally at the lower lateral edge of the putamen (B); demyelination (D) and astrogliosis (F) is observed in patient No. 67 when compared with a control subject (C, E); lacunar infarction at the lower end of the extreme capsule and insular cortex (G); and old subinsular hemorrhage (H). The filled asterisks indicate the extreme capsule and open asterisks indicate the external capsule (C–F). Bars indicate 500 μm (A–D), 200 μm (E, F) and 2 mm (G, H).

the OND and non-neurological control groups in the consecutive autopsy brains. A significantly higher age in the CVD group may have strengthened these WM lesions, as WM lesions are known to be strongly associated with aging. The neuropathological changes were common to those seen in the periventricular

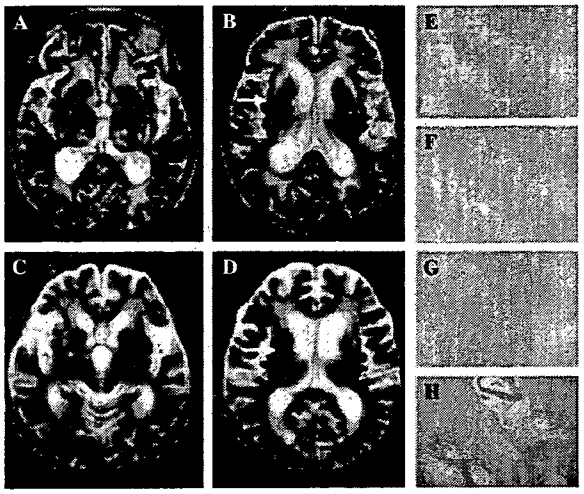

Figure 3. MR images of SIVD patients (A and B from patient No. 58, C and D from patient No. 67) and photomicrographs of Klüver–Barrera staining in the external capsule (E from a control subject, F from patient No. 58, G from patient No. 67) and H&E staining in the lower lateral edge of the putamen (H from patient No. 67). The arrows in (B) and (D) indicate the corresponding regions in (F) and (G), respectively. Note that the subinsular hyperintensities are severe in (A, B) and mild in (C, D). Patient No. 58 had obvious demyelination (F) when compared with the control (E), whereas in patient No. 67, the demyelination was mild (G) with a dilated perivascular space in the subinsular region at the lower putamen level (H).

WM, supplementing the notion that subinsular WM lesions are continuum of the periventricular WM lesions in a previous CT study [17].

Demyelination and gliosis of the WM can be experimentally induced by chronic cerebral hypoperfusion in rodents, supplementing that this type of WM lesions are caused by chronic cerebral ischemia [18–20]. In addition, cerebral edema may be another causative mechanism leading to WM lesions. Extravasated edema fluid is transported into the vascular systems in the periventricular WM, and is finally drained into the ventricular CSF. Thus, subinsular WM lesions may be pathogenetically attributable to chronic cerebral ischemia and/or cerebral edema.

In previous studies, another types of lesions except for demyelination and gliosis have been also reported in the subinsular region. A postmortem MR imaging study revealed that subinsular hyperintensities corresponded to dilated perivascular spaces in the lower portion of the extreme capsule [10]. Furthermore, a single dilated perivascular space appeared as a large hyperintense spot in the lower lateral edge of the putamen [21,22]. In concordance with these results, the dilated perivascular space was found in the lower one-third of the extreme capsule and the lower lateral edge of the putamen. The insular arteries penetrate and course medio-superiorly toward the claustrum in the lower one-third of the extreme capsule. On the contrary, the lateral lenticulostriate arteries penetrate and turn dorsally in the lower lateral edge of the putamen. Dilated perivascular space is reported to show punctate hyperintensities, whereas demyelination is more likely to correspond to extensive ill-defined lesions [23].

Thus, the present study demonstrated two types of subinsular lesions: demyelination and gliosis extending from the anterior periventricular WM lesions at the mid-putamen level; and dilated perivascular spaces at the lower putamen level. In clinical practice, insular stroke restricted to the insular cortex is exceptional [24]. The present series also included only one patient with either subinsular lacunar infarction or hemorrhage, indicating that a focal lesion is extremely rare in this region. Although the radiological features of subinsular lacunar infarction remain unclear, it is expected that subinsular hyperintensities most likely reflect demyelination, gliosis and a dilated perivascular space from the viewpoint of the frequency of these neuropathological substrates.

In conclusion, subinsular T2 hyperintensities rarely correspond to lacunar infarction or cerebral hemorrhage, but correspond to demyelination and gliosis at the mid-putamen level, and dilated perivascular spaces at the lower putamen level.

Acknowledgments

This work was supported by grants from the Ministry of Education, Culture, Sports, Science and Technology, Japan (H. T.). We are indebted to Miss Hitomi Nakabayashi for her excellent technical assistance.

References

1. Kier EL, Staib LH, Davis LM, Bronen RA. MR Imaging of the temporal stem: anatomic dissection tractography of the uncinate fasciculus, inferior occipitofrontal fasciculus, and Meyer's loop of the optic radiation. *American Journal of Neuroradiology* 2004; **25:** 677–691.
2. Selden NR, Gitelman DR, Salamon-Murayama N, Parrish TB, Mesulam MM. Trajectories of cholinergic pathways within the cerebral hemispheres of the human brain. *Brain* 1998; **121:** 2249–2257.
3. Wallin A, Alafuzoff I, Carlsson A, *et al.* Neurotransmitter deficits in a non-multi-infarct category of vascular dementia. *Acta Neurologica Scandinavica* 1989; **79:** 397–406.
4. Swartz RH, Sahlas DJ, Black SE. Strategic involvement of cholinergic pathways and executive dysfunction: does location of white matter signal hyperintensities matter? *Journal of Stroke and Cerebrovascular Disease* 2003; **12:** 29–36.
5. Tomimoto H, Ohtani R, Shibata M, Nakamura N, Ihara M. Loss of cholinergic pathway in vascular dementia of

the Binswanger type. *Dementia Geriatric Cognitive Disorders* 2005; **19:** 282–288.
6. Mesulam M, Siddique T, Cohen B. Cholinergic denervation in a pure multi-infarct state: observations on CADASIL. *Neurology* 2003; **60:** 1183–1185.
7. Marinkovic R, Markovic L. The role of the middle cerebral artery in the vascularization of the claustrum. *Medicinski Pregled* 1990; **43:** 361–365.
8. Ture U, Yasargil MG, Al-Mefty O, Yasargil DC. Arteries of the insula. *Journal of Neurosurgery* 2000; **92:** 676–687.
9. van Den Boom R, Lesnik Oberstein SA, van Duinen SG, *et al.* Subcortical lacunar lesions: an MR imaging finding in patients with cerebral autosomal dominant arteriopathy with subcortical infarcts and leukoencephalopathy. *Radiology* 2002; **224:** 791–796.
10. Song CJ, Kim JH, Kier EL, Bronen RA. MR imaging and histologic features of subinsular bright spots on T2-weighted MR images: Virchow-Robin spaces of the extreme capsule and insular cortex. *Radiology* 2000; **214:** 671–677.
11. Bennett DA, Wilson RS, Gilley DW, Fox JH. Clinical diagnosis of Binswanger's disease. *Journal of Neurology, Neurosurgery and Psychiatry* 1990; **53:** 961–965.
12. Fazekas F, Kleinert R, Offenbacher H, *et al.* The morphologic correlate of incidental punctate white matter hyperintensities on MR images. *American Journal of Neuroradiology* 1991; **12:** 915–921.
13. Auer DP, Putz B, Gossl C, *et al.* Differential lesion patterns in CADASIL and sporadic subcortical arteriosclerotic encephalopathy: MR imaging study with statistical parametric group comparison. *Radiology* 2001; **218:** 443–451.
14. O'Sullivan M, Jarosz JM, Martin RJ, *et al.* MRI hyperintensities of the temporal lobe and external capsule in patients with CADASIL. *Neurology* 2001; **56:** 628–634.
15. Markus HS, Martin RJ, Simpson MA, *et al.* Diagnostic strategies in CADASIL. *Neurology* 2002; **59:** 1134–1138.
16. Tomimoto H, Ohtani R, Wakita H, *et al.* Small artery dementia in Japan; radiological differences between CADASIL, leukoaraiosis and Binswanger's disease. *Dementia Geriatric Cognitive Disorders* 2006; **21:** 162–169.
17. Cobb SR, Mehringer CM, Itabashi HH, Pribram H. CT of subinsular infarction and ischemia. *American Journal of Neuroradiology* 1987; **8:** 221–227.
18. Shibata M, Ohtani R, Ihara M, Tomimoto H. White matter lesions and glial activation in a novel mouse model of chronic cerebral hypoperfusion. *Stroke* 2004; **35:** 2598–2603.
19. Wakita H, Tomimoto H, Akiguchi I, Kimura J. Glial activation and white matter changes in the rat brain induced by chronic cerebral hypoperfusion: an immunohistochemical study. *Acta Neuropathologica (Berlin)* 1994; **87:** 484–492.
20. Roman GC. Brain hypoperfusion: a critical factor in vascular dementia. *Neurology Research* 2004; **26:** 454–458.
21. Poirier J. Giant cerebral lacuna due to dilatation of the perivascular space: a case report. *Clinical Neuropathology* 1983; **2:** 138–140.
22. Pullicino PM, Miller LL, Alexandrov AV, Ostrow PT. Infraputaminal 'lacunes'. Clinical and pathological correlations. *Stroke* 1995; **26:** 1598–1602.
23. Munoz DG, Hastak SM, Harper B, Lee D, Hachinski VC. Pathologic correlates of increased signals of the centrum ovale on magnetic resonance imaging. *Archives of Neurology* 1993; **50:** 492–497.
24. Cereda C, Ghika J, Maeder P, Bogousslavsky J. Strokes restricted to the insular cortex. *Neurology* 2002; **59:** 1950–1955.

Available online at www.sciencedirect.com
ScienceDirect
Diabetes Research and Clinical Practice 76 (2007) 12–17
DIABETES RESEARCH AND CLINICAL PRACTICE
www.elsevier.com/locate/diabres

Association between insulin resistance and endothelial dysfunction in type 2 diabetes and the effects of pioglitazone

Masaaki Suzuki [a,*], Itaru Takamisawa [b], Yasunao Yoshimasa [b], Yutaka Harano [c]

[a] *Department of Diabetes and Metabolic Disease, Osaka General Medical Center, 3-1-56 Mandai-higashi, Sumiyoshi-ku, Osaka 558-8558, Japan*
[b] *Division of Diabetes and Atherosclerosis, Department of Medicine, National Cardiovascular Center, Japan*
[c] *Department of Nutrition, Koshien Univesity College of Nutrition, Japan*

Received 25 July 2005; received in revised form 5 June 2006; accepted 28 July 2006
Available online 27 September 2006

Abstract

Endothelial dysfunction is regarded as an early stage of atherosclerosis, and plays a role in the development of atherosclerotic diseases. Insulin resistance is related to the atherosclerotic process. In this study, we examined the association between endothelial function and insulin resistance in 48 subjects with type 2 diabetes. In addition, the effects of pioglitazone treatment on endothelial function and insulin resistance were investigated in a subgroup of subjects. Endothelial function of the brachial artery was non-invasively assessed using ultrasound technique. We measured flow-mediated endothelium-dependent vasodilation (FMD) and glyceryl trinitrate-induced endothelium-independent vasodilation (GTN). Insulin sensitivity was measured by the steady-state plasma glucose (SSPG) method. High SSPG levels indicate insulin resistance. There was a significant inverse correlation ($r = -0.462$, $p < 0.001$) between SSPG and FMD. Systolic blood pressure was inversely correlated with FMD ($r = -0.360$, $p < 0.013$). By multiple regression analysis, insulin resistance was the sole predictor of FMD. The effects of chronic treatment with pioglitazone were assessed in 10 subjects with type 2 diabetes. The increase in FMD significantly correlated with the decrease in SSPG. There is a significant association between vascular endothelial dysfunction and insulin resistance in type 2 diabetes. This result was supported by the effects of the insulin sensitizer, pioglitazone.

Keywords: Endothelial dysfunction; Insulin resistance; Pioglitazone

1. Introduction

Endothelial dysfunction is thought to be an important early feature in the development of atherosclerosis and occurs in subjects with type 2 diabetes mellitus [1–4]. Insulin resistance is also associated with atherosclerosis and is observed in subjects with type 2 diabetes [5,6]. We previously reported the association between endothelial dysfunction and insulin resistance in patients with essential hypertension [7]. However, the mechanisms responsible for endothelial dysfunction and insulin resistance in hypertension might be different from those of type 2 diabetes. Therefore, we evaluated the relationship between endothelial dysfunction and insulin resistance in patients with type 2 diabetes. Thiazolidinediones, an agonist for the peroxisome proliferator-activated receptor γ (PPARγ), improve insulin resistance. If there is a significant relationship

* Corresponding author. Tel.: +81 6 6692 1201; fax: +81 6 6606 7000.
E-mail address: masuzuki@gh.pref.osaka.jp (M. Suzuki).

0168-8227/$ – see front matter © 2006 Elsevier Ireland Ltd. All rights reserved.
doi:10.1016/j.diabres.2006.07.033

between endothelial dysfunction and insulin resistance, thiazolidinediones might influence endothelial function. Therefore, we examined the effects of pioglitazone on endothelial dysfunction and insulin resistance in a subgroup of subjects with type 2 diabetes to verify the relationship between endothelial dysfunction and insulin resistance.

The main purpose of this study was to investigate the relation between vascular endothelial dysfunction and insulin resistance in type 2 diabetes. In addition, the influence of pioglitazone treatment was examined.

2. Subjects and methods

2.1. Subjects

Forty-eight (30 males and 18 females) patients with type 2 diabetes were recruited in the Department of Diabetes and Atherosclerosis of the National Cardiovascular Center. The subjects did not have diabetic retinopathy or nephropathy. Subjects were included on the basis of the following criteria: age between 40 and 79 years, body mass index (BMI) between 17 and 35 kg/m^2, type 2 diabetes confirmed by American Diabetes Association criteria [8]. Subjects were excluded from participation if they had coronary heart, peripheral vascular, renal, hepatic or other endocrine diseases. Subjects were excluded if they had a resting seated blood pressure greater than 150 mmHg systolic or greater than 90 mmHg diastolic, or were taking anti-hypertensive drugs. Diabetes duration was 5.3 ± 1.9 years (3–7 years). Diabetes treatment regimens included diet alone (27 subjects), sulfonylures (18 subjects) and metformin (3 subjects).

The 48 subjects had an average age of 64 ± 1 years, with a mean BMI of 24.6 ± 0.3 kg/m^2, HbA_{1c} of 8.6 ± 0.2%, total cholesterol of 199 ± 5 mg/dl, HDL-cholesterol of 43 ± 2 mg/dl and triglycerides of 137 ± 14 mg/dl. Mean systolic and diastolic blood pressures were 131 ± 3 and 74 ± 2 mmHg, respectively.

Of the 48 diabetic subjects, 10 subjects were started on a single 15 or 30 mg-tablet of pioglitazone (Actos, Takeda Pharmaceuticals, Tokyo, Japan) by mouth each day. Inclusion criteria of the pioglitazone treatment were male, non-smoker, diet alone treatment and mild to severe insulin resistance (SSPG > 160 mg/dl). They received a mean dose of 25.5 ± 2.3 mg/day (30 mg/day: seven subjects and 15 mg/day: three subjects) of pioglitazone for 16.3 ± 1.6 weeks (10–20 weeks). The secondary assessments of endothelial function and insulin sensitivity were performed after the pioglitazone treatments.

The study protocol was approved by the ethics committee of the National Cardiovascular Center. The experiments were conducted with the understanding and the consent of each participant.

2.2. Methods

2.2.1. Assessment of endothelial function

Using the ultrasound method, arterial endothelium and smooth muscle function were measured by examining brachial artery responses to endothelium-dependent and endothelium-independent stimuli. Ultrasound measurements were carried out based on the method described by Celermajer et al. [9] and our method was reported previously [7]. The assessments were performed after an overnight fast in a quiet air-conditioned room (22–23 °C). The diameter of the brachial artery was measured on B-mode ultrasound images, with the use of a 10-MHz linear array transducer (ProSound SSD-5500, ALOKA, Tokyo, Japan). The right brachial artery was scanned in longitudinal sections 1–10 cm above the elbow, after at least 15 min of rest in the supine position. After the detection of the right transducer position, the skin surface was marked and the arm was kept in the same position during the study. All scans were recorded using a super-VHS videocassette recorder (SONY, SVO-9500MD), and analyzed later.

At first, baseline measurements of the diameter were carried out. Endothelium-dependent vasodilation (flow-mediated dilation) was determined by the scans during reactive hyperemia. Because flow-mediated vasodilation was mainly blocked by *N*-monomethyl-L-arginine (an inhibitor of endothelial nitric oxide synthase) this dilation was regarded as endothelium dependent [10]. A pneumatic cuff placed around the forearm was inflated to 220 mmHg and was deflated after 4.5 min. The diameter of the brachial artery was scanned and recorded after deflation. After 10–15 min rest, the second control scan of the diameter and the flow velocity was recorded. Then, sublingual glyceryl trinitrate spray (300 μg) was administered and 3.5–4 min later a final scan of the diameter was recorded.

Measurements of the vessel diameter were taken from the anterior to the posterior 'm' line (interface between the media and adventitia) at endo-diastole, coincident with the R wave on a continuously recorded electrocardiogram. The diameters at four cardiac cycles were measured for each scan, and these results were averaged. Determinations of the flow-mediated dilation were carried out 45–60 s after the cuff release to measure a maximum diameter. Vasodilation by reactive hyperemia (flow-mediated dilation, FMD) or glyceryl trinitrate (GTN) was expressed as the percent change in diameter compared to the baseline values.

2.2.2. Insulin sensitivity test

Glucose utilization in response to insulin was evaluated by a modified steady state plasma glucose (SSPG) method [6,7,11] using Sandostatin (octreotide acetate; Novartis, Basel, Switzerland) after an overnight fasting for at least 12 h. Sandostatin (9.8 pmol in bolus followed by a constant infusion of 73.5 pmol/h) and Novolin R insulin (Novo Nordisk S/A, Tokyo, Japan, 45 pmol/kg [7.5 mU/kg] in a bolus followed by a constant infusion at a rate of 4.62 pmol/kg/min [0.77 mU/kg/min]) were infused intravenously for 120 min.

Glucose in a final 12% solution containing KCl (0.5 μmol/kg/min) were infused at a rate of 0.033 mmol/kg/min [6 mg/kg/min] through an antecubital vein via a constant infusion pump. Blood samples were drawn routinely at 0 and 120 min (9:00 and 11:00 a.m.) for determination of glucose and insulin. Value of glucose at 120 min (SSPG) was used as a marker of insulin sensitivity to glucose utilization. High SSPG levels indicate peripheral insulin resistance. At 120 min SSPG was rapidly measured using a Glucometer (Bayer Corporation, Osaka, Japan) separate from the usual measurement of glucose and insulin. When rapidly measured, if SSPG was found to be lower than 250 mg/dl, oral glucose intake was necessary to prevent hypoglycemia after the insulin sensitivity test. The subjects should have lunch within 30 min after the insulin sensitivity test to prevent hypoglycemia. Homeostasis model assessment (HOMA-IR) was calculated from fasting glucose and insulin concentrations during insulin sensitivity test as follows: HOMA-IR = fasting glucose (mg/dl) × fasting insulin (μU/ml)/405.

2.3. Statistical analysis

Values are expressed as mean ± S.E. A probability value of <0.05 was considered to indicate statistical significance. The strength of the correlation between FMD and GTN with respect to risk factors was assessed by Pearson's linear correlation and multiple regression analysis. The effects of pioglitazone on each clinical parameter were assessed by paired *t*-test and Pearson's linear correlation.

3. Results

3.1. Association between endothelial dysfunction and each parameter in 48 subjects

A significant inverse correlation was observed between FMD and SSPG ($r = -0.462$, $p < 0.001$; Fig. 1). There was no relation between FMD and HbA_{1c} ($p = 0.856$). We also observed a significant inverse correlation between FMD and systolic blood pressure ($r = -0.360$, $p < 0.013$). No significant correlation was found between FMD and diabetic duration, diastolic blood pressure, total cholesterol, HDL cholesterol, triglyceride, age or BMI. There was no relationship between FMD and HOMA-IR ($p = 0.097$).

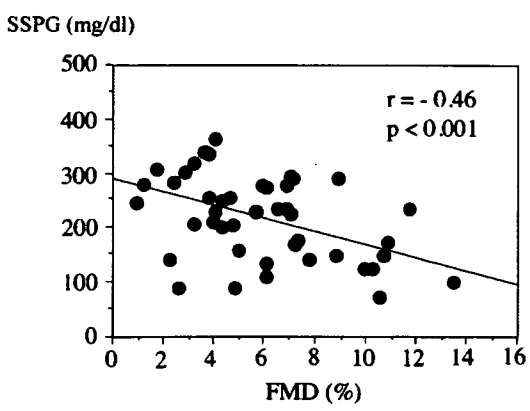

Fig. 1. Relationship between FMD and SSPG in subjects with type 2 diabetes. FMD, flow-mediated vasodilation; SSPG, steady state plasma glucose.

We performed multiple regression analysis to evaluate the independent influence of risk factors including SSPG, systolic blood pressure, HbA_{1c}, total cholesterol, BMI and age on FMD. FMD was independently related to SSPG (regression coefficient:$\beta = -0.419$, $p = 0.0086$) but not to systolic blood pressure ($\beta = -0.254$, $p = 0.0782$), HbA_{1c} ($\beta = -0.090$, $p = 0.5616$), total cholesterol ($\beta = -0.067$, $p = 0.6336$), BMI ($\beta = -0.258$, $p = 0.0863$) or age ($\beta = -0.085$, $p = 0.5650$).

With respect to GTN, no significant correlation was observed between GTN and SSPG or other parameters, including HbA_{1c}, diabetic duration, systolic blood pressure, diastolic blood pressure, total cholesterol, HDL cholesterol, triglyceride, age or BMI.

3.2. Effects of pioglitazone treatment on endothelial function and insulin resistance

The effects of treatment with pioglitazone were assessed in 10 male subjects with type 2 diabetes (a subgroup of 48 subjects). Table 1 shows the clinical parameters of the 10 subjects before and after pioglitazone treatment. SSPG, HbA_{1c} and fasting plasma glucose decreased and FMD increased significantly due to pioglitazone treatment. However, BMI, total cholesterol, HDL-cholesterol, triglyceride, systolic blood pressure and diastolic blood pressure did not

Table 1
Clinical characteristics of the subjects with type 2 diabetes treated with pioglitazone

	Before Tx	After Tx
Number	10	
Age (years)	65 ± 2	
SSPG (mg/dl)	230 ± 13	185 ± 17*
FMD (%)	4.5 ± 1.1	8.1 ± 1.5***
Body mass index (kg/m^2)	24.4 ± 0.4	24.7 ± 0.4
Fasting plasma glucose (mg/dl)	162 ± 11	133 ± 8*
HbA_{1c} (%)	8.4 ± 0.4	7.0 ± 0.3**
Total cholesterol (mg/dl)	199 ± 8	206 ± 7
HDL cholesterol (mg/dl)	47 ± 4	50 ± 4
Triglyceride (mg/dl)	120 ± 15	129 ± 13
Systolic blood pressure (mmHg)	137 ± 5	137 ± 2
Diastolic blood pressure (mmHg)	78 ± 5	79 ± 1

Values are mean ± S.E. *$p < 0.05$, **$p < 0.01$, ***$p < 0.001$ vs. before Tx. Tx, Treatments with pioglytazone.

significantly change. GTN was also not significantly altered.

The change in FMD before and after administration of pioglitazone was not significantly correlated with the change in HbA_{1c} ($p = 0.314$) or fasting plasma glucose ($p = 0.717$). The increase in FMD, that is, the improvement in endothelial function, was significantly correlated with the decrease in SSPG ($r = -0.649$, $p < 0.05$).

4. Discussion

In this study we found that vascular endothelial dysfunction was associated with insulin resistance in type 2 diabetes. This result was supported by the effects of the insulin sensitizer, pioglitazone, which improved both endothelial dysfunction and insulin resistance in patients with type 2 diabetes.

The close association between insulin resistance and endothelial dysfunction is our main interest. In a study by Hogikyan et al. [3], insulin resistance as measured by the insulin sensitivity index (minimal model: S_I), was not found to be correlated with endothelial dysfunction in subjects with type 2 diabetes. They measured the forearm blood flow (FABF) using venous occlusion plethysmography and used the FABF response to acetylcholine as an index of endothelial function. The narrow range of S_I values among the subjects might have led to the lack of a relationship between S_I and endothelial dysfunction. In addition, the sensitivity of the techniques using plethysmography might have been low.

Balletshofer et al. [12] reported a significant association between endothelial dysfunction and insulin resistance, as measured by the glucose clamp method, in young normotensive and normoglycemic first-degree relatives of patients with type 2 diabetes. Therefore, this association was observed in a non-diabetic population at future risk of type 2 diabetes.

Insulin causes endothelium-derived nitric oxide (NO)-dependent vasodilation [13]. It is suggested that this insulin action occurs via the phosphatidylinositol 3-kinase and Akt pathway [14,15]. As for insulin action, phosphatidylinositol 3-kinase activation is critical for insulin-mediated glucose uptake into skeletal muscle [16]. Therefore, insulin resistance due to a systemic defect in the phosphatidylinositol 3-kinase pathway might cause a combined defect in insulin-mediated glucose uptake and insulin-mediated endothelial vasodilation.

Among the risk factors for atherosclerosis, insulin resistance was found to be the sole predictor of endothelium dependent vasodilation by multiple regression analysis in the present study. We observed no relationship between FMD and HbA_{1c}. Bagg et al. found that a short-term reduction of HbA_{1c} levels did not appear to affect endothelial function in patients with type 2 diabetes [17]. Furthermore, Mather et al. reported that insulin resistance was the sole predictor of endothelial dysfunction following metformin treatment in type 2 diabetes in stepwise multivariate analysis, and HbA_{1c} and glucose levels were not significant predictors of endothelial dysfunction [18].

Treatment with HMG-CoA inhibitors (statins) has been shown to improve endothelial dysfunction [19–21]. Therefore, statin treatment may have affected the relationship between FMD and risk factors in the present study. In 48 diabetic subjects, 5 were treated with pravastatin and one with simvastatin. We performed statistical analysis in 42 subjects without statin treatment. There was a significant inverse correlation between SSPG and FMD ($r = -0.538$, $p < 0.001$). A significant inverse correlation was observed between FMD and systolic blood pressure ($r = -0.330$, $p < 0.05$). No significant correlation was found between FMD and HbA_{1c}, diabetic duration, diastolic blood pressure, total cholesterol, HDL cholesterol, triglyceride, age or BMI. On multiple regression analysis, FMD was independently related to SSPG (regression coefficient: $\beta = -0.500$, $p = 0.0032$) but not to systolic blood pressure, HbA_{1c}, total cholesterol, BMI or age.

Smoking is associated with endothelial dysfunction [22,23]. Smoking might interfere in the relationship between FMD and risk factors. In 48 diabetic subjects, 13 were smokers in the present study. Statistical analysis was performed in 35 non-smokers. A significant correlation was found between SSPG and FMD ($r = -0.582$, $p < 0.001$). There was a significant inverse correlation between FMD and systolic blood pressure ($r = -0.357$, $p < 0.05$). No significant correlation was observed between FMD and HbA_{1c}, diabetic duration, diastolic blood pressure, total cholesterol, HDL cholesterol, triglyceride, age or BMI. On multiple regression analysis, FMD was independently related to SSPG (regression coefficient: $\beta = -0.591$, $p = 0.0019$) but not to systolic blood pressure, HbA_{1c}, total cholesterol, BMI or age. In the present study, FMD did not correlate with HOMA-IR. SSPG is a more sensitive marker to measure insulin sensitivity than HOMA-IR.

Endothelial dysfunction and insulin resistance were improved by pioglitazone treatment in the present study. SSPG, HbA_{1c} and fasting plasma glucose were decreased and other risk factors were not changed by the treatment. It was reported that hyperglycemia itself inhibits endothelial NO synthase activity [24] and causes endothelial dysfunction [25]. On the other hand,

insulin resistance was also associated with endothelial dysfunction in 48 subjects with type 2 diabetes in this study. The change in FMD before and after treatment with pioglitazone was not significantly correlated with the change in HbA_{1c} or fasting plasma glucose, and the increase in FMD was significantly correlated with the decrease in SSPG in this study. Because of the small number of subjects ($n = 10$), we cannot exclude the possibility that the decreased plasma glucose level improved endothelial dysfunction. The decrease in plasma glucose level might be associated with improved endothelial function if the pioglitazone study was performed with more cases. It can at least be said that insulin resistance is an important factor affecting endothelial function. As previously described, a similar study [18] found that treatment with metformin improved both endothelial function and insulin resistance, and the glucose level and HbA_{1c} were not significant predictors of endothelial dysfunction. Considering generally than the above-mentioned points, it is suggested that increased insulin sensitivity plays an important role in the improvement of endothelial function by pioglitazone treatment.

Pistrosch et al. [26] demonstrated that treatment with rosiglitazone, another PPARγ activator, ameliorated insulin resistance measured by glucose clamp method, and improved endothelial function determined by venous occlusion plethysmography in patients with recently diagnosed type 2 diabetes. They performed a double-blind cross-over trial and treated with rosiglitazone and nateglinide in random order. Glycemic control was comparable under rosiglitazone and nateglinide. Only rosiglitazone improved insulin resistance and endothelial function in the study. Thus, they also showed the relation between insulin sensitivity and endothelial function independent of glucose level in type 2 diabetes.

In conclusion, in the present study we demonstrated significant association between vascular endothelial dysfunction and insulin resistance in type 2 diabetes, and pioglitazone treatment improved both endothelial dysfunction and insulin resistance with a statistical link. These data support the concept of the important role of insulin resistance in the pathogenesis of endothelial dysfunction in type 2 diabetes mellitus.

References

[1] S.B. Williams, J.A. Cusco, M.A. Roddy, M.T. Johnstone, M.A. Creager, Impaired nitric oxide-mediated vasodilation in patients with non-insulin-dependent diabetes mellitus, J. Am. Coll. Cardiol. 27 (1996) 567–574.

[2] A. Avogaro, F. Piarulli, A. Valerio, M. Miola, M. Calveri, P. Pavan, et al., Forearm nitric oxide balance, vascular relaxation, and glucose metabolism in NIDDM patients, Diabetes 46 (1997) 1040–1046.

[3] R.V. Hogikyan, A.T. Galecki, B. Pitt, J.B. Halter, D.A. Greene, M.A. Supiano, Specific impairment of endothelium-dependent vasodilation in subjects with type 2 diabetes independent of obesity, J. Clin. Endocrinol. Metab. 83 (1998) 1946–1952.

[4] M.A. Creager, T.F. Luscher, F. Cosentino, J.A. Beckman, Diabetes and vascular disease: pathophysiology, clinical consequences, and medical therapy: part I, Circulation 108 (2003) 1527–1532.

[5] K. Shinozaki, M. Suzuki, M. Ikebuchi, Y. Hara, Y. Harano, Demonstration of insulin resistance in coronary heart disease documented with angiography, Diabetes Care 19 (1996) 1–7.

[6] Y. Harano, S. Ohgaku, K. Kosugi, H. Yasuda, T. Nakano, M. Kobayashi, et al., Clinical significance of altered insulin sensitivity in diabetes mellitus assessed by glucose, insulin and somatostatin infusion, J. Clin. Endocrinol. Metab. 52 (1981) 982–987.

[7] M. Suzuki, I. Takamisawa, K. Suzuki, A. Hiuge, T. Horio, Y. Yoshimasa, et al., Close association of endothelial dysfunction with insulin resistance and carotid wall thickening in hypertension, Am. J. Hypertens. 17 (2004) 228–232.

[8] Report of the Expert Committee on the Diagnosis and Classification of Diabetes Mellitus, Diabetes Care 26 (Suppl. 1), 2002, pp. S4–S19.

[9] D.S. Celermajer, K.E. Sorensen, V.M. Gooch, D.J. Spiegelhalter, O.I. Miller, I.D. Sullivan, et al., Non-invasive detection of endothelial dysfunction in children and adults at risk of atherosclerosis, Lancet 340 (1992) 1111–1115.

[10] R. Joannides, W.E. Haefeli, L. Linder, V. Richard, E.H. Bakkali, C. Thuillez, et al., Nitric oxide is responsible for flow-dependent dilatation of human peripheral conduit arteries in vivo, Circulation 91 (1995) 1314–1319.

[11] M. Ikebuchi, M. Suzuki, A. Kageyama, J. Hirose, C. Yokota, K. Ikeda, et al., Modified method using a somatostatin analogue, octreotide acetate (Sandostatin®) to assess in vivo insulin sensitivity, Endocr. J. 43 (1996) 125–130.

[12] B.M. Balletshofer, K. Rittig, M.D. Enderle, A. Volk, E. Maerker, S. Jacob, et al., Endothelial dysfunction is detectable in young normotensive first-degree relatives of subjects with type 2 diabetes in association with insulin resistance, Circulation 101 (2000) 1780–1784.

[13] C. Cardillo, S.S. Nambi, C.M. Kilcoyne, W.K. Choucair, A. Katz, M.J. Quon, et al., Insulin stimulates both endothelin and nitric oxide activity in the human forearm, Circulation 100 (1999) 820–825.

[14] W.A. Hsueh, R.E. Law, 1999 Insulin signaling in the arterial wall, Am. J. Cardiol. 84 (1999) 21J–24J.

[15] G. Zeng, F.H. Nystrom, L.V. Ravichandran, Li-Na. Cong, M. Kirby, H. Mostowski, et al., Roles for insulin receptor, PI3-kinase, and Akt in insulin-signaling pathways related to production of nitric oxide in human vascular endothelial cells, Circulation 101 (2000) 1539–1545.

[16] P.R. Shepherd, D.J. Withers, K. Siddle, Phosphatidylinositol 3-kinase: the key switch mechanism in insulin signaling, Biochem. J. 333 (1998) 471–490.

[17] W. Bagg, G.A. Whalley, G. Gamble, P.L. Drury, N. Sharpe, G.D. Braatvedt, Effects of improved glycaemic control on endothelial function in patients with type 2 diabetes, Intern. Med. J. 31 (2001) 322–328.